Journal of Alloys and Compounds 509 (2011) 5919–5925

Contents lists available at ScienceDirect

Journal of Alloys and Compounds

journal homepage: www.elsevier.com/locate/jallcom

# Influences of cobalt substitution and size effects on magnetic properties of coprecipitated Co–Fe ferrite nanoparticles

Nguyen Thi Lan, Nguyen Phuc Duong*, Than Duc Hien

*International Training Institute for Materials Science (ITIMS), Hanoi University of Technology, 1 Dai Co Viet Road, Hanoi, Viet nam*

ARTICLE INFO

*Article history:*
Received 15 February 2011
Received in revised form 4 March 2011
Accepted 4 March 2011
Available online 12 March 2011

*Keywords:*
Spinel ferrite
Cobalt substitution
Nanoparticles
Magnetic properties
Superparamagnetic
Finite size effects

ABSTRACT

Co-substituted ferrite nanoparticles with narrow size distribution have been prepared by coprecipitation method. X-ray diffraction (XRD) showed that the samples have cubic spinel structure of which the lattice constant slightly decreases upon cobalt substitution. The mean crystallite size of the samples was in the range 9.5–11 nm as deduced from the XRD line broadening. Energy dispersive X-ray spectroscopy (EDX) verified the presence of cobalt in the substituted samples. The morphology and size distribution of the nanoparticles were studied using transmission electron microscopy (TEM). Magnetic properties were determined using a vibrating sample magnetometer (VSM). The samples are characterized by a superparamagnetic transition at blocking temperatures $T_B$ below room temperature. The coercivity $H_c$ at low temperatures follows a simple model of thermal activation of particle's moment over the anisotropy barrier in the temperature range below $T_B$ which is in accordance with Kneller's law for ferromagnetic materials. From the blocking temperature and from the thermal decay of the coercivity, the effective anisotropy constant values were determined to be in order of $10^6$ erg/cm$^3$. The Curie temperature $T_C$ and saturation magnetization $M_s$ at nanoscale are lower than those of the bulk and decrease with the increase of cobalt content.



## 1. Introduction

Spinel ferrite nanoparticles have been a subject of interest in recent years due to their promising technological applications such as high-density recording devices, ferrofluids and biomedicine [1–3] and to understand how bulk properties transform to the atomic as the size is decreased. Nanosized ferrite particles exhibit unusual magnetic properties which are not observed in the bulk material, e.g. single domain behavior, superparamagnetism, and reduced Curie temperature and magnetization [4–6]. The spatial confinement at nanoscale enhances the role of surface atoms with reduced symmetry and the consequent larger number of broken exchange bonds can result in surface anisotropy, frustration and spin disorder [7]. Superparamagnetism is a unique and important feature of magnetism in the nanosized magnetic particles. When the magnetic anisotropy energy of a single domain magnetic nanoparticle ($\sim KV$, where $K$ is the anisotropy constant and $V$ is the volume of the particle) becomes comparable to thermal activation energy $k_BT$, where $k_B$ is Boltzmann's constant, the magnetization direction starts flipping randomly and goes through rapid superparamagnetic relaxation. The temperature above which the thermal activation energy overcomes the magnetic anisotropy energy barrier and the nanoparticle becomes superparamagnetic is known as the blocking temperature $T_B$. Understanding and controlling the superparamagnetic features of the ferrite nanoparticles are important for many applications. On the other hand, modifications of the magnetic properties of ferrites in the bulk and nanosized forms can also be carried out via substitution of other 3d ions for iron [8–10]. For instance, cobalt substitution strongly enhances the magnetocrystalline anisotropy of the spinel ferrites (see e.g. [8]). It is therefore interesting to study the competition between the crystal anisotropy and other sources of anisotropy in these spinel ferrite nanoparticles and their influences in the superparamagnetic behavior.

In this work we have studied the cobalt substitution and size effects on the magnetic properties of $Co_xFe_{3-x}O_4$ nanoparticles, in particular the superparamagnetic transition and the effective magnetic anisotropy energy.

## 2. Experimental

Nanoparticles of $Co_xFe_{3-x}O_4$ were synthesized by coprecipitating chlorides of $Fe^{3+}$, $Fe^{2+}$ and $Co^{2+}$ cations in aqueous solution with pH ≈ 7. Sodium hydroxide, NaOH, was used as the reaction agent. Starting chemicals were of analytical grade. In order to obtain spinel ferrite phases containing cobalt, the precipitation process has been carried out at temperature near 280 K. The particles were washed many times with distilled water followed by acetone rinse and dry at room temperature. Three samples S0, S02 and S04 were obtained with

* Corresponding author. Tel.: +84 4 38680787; fax: +84 4 38692963.
*E-mail address:* duong@itims.edu.vn (N.P. Duong).

0925-8388/$ – see front matter © 2011 Elsevier B.V. All rights reserved.
doi:10.1016/j.jallcom.2011.03.050

the input ratios of the divalent cations $[Co^{2+}]/[Fe^{2+}]$ equal to 0, 0.2 and 0.4, respectively.

The crystal structure, particle size and morphology of the dried precipitates were determined by X-ray diffraction (XRD), transmission electron microscopy (TEM) measurements at room temperature. The elemental characterization was carried out by using energy dispersive X-ray spectroscopy (EDX).

Magnetic properties of the samples were studied at temperatures from 100 K to 700 K and in applied fields $H$ up to 12 kOe using a vibrating sample magnetometer (VSM). For magnetic measurements below room temperature, nanoparticles were fixed in a solid matrix of stycast epoxy. Amounts of nanoparticles and epoxy were prepared with the mass ratio of particles and epoxy of approximately 1:9. The epoxy was first heated and became liquidized at ~75 °C. The nanoparticles were then added and dispersed in the molten epoxy by using ultrasonic for 30 min. The mixture became solidified after 24 h. For thermomagnetic measurements, the nanoparticles were pressed into the forms of pellets.

## 3. Results and discussion

### 3.1. Structural, morphology and composition characterization

The cobalt content in the samples was obtained by EDX. Analysis was carried out at 8 different points of each sample. The compositions at different positions for all cases are very close to one and another. Table 1 shows the average values of $x$ which match well with the formula percentage of the ferrites.

Fig. 1 shows the XRD patterns for as-precipitated $Co_xFe_{3-x}O_4$ powders. The data indicate the crystallization of the samples in the spinel structure. The lattice parameter $a$ is determined from the XRD patterns and listed in Table 1. For $x = 0$, a value of 8.398 Å was found for $a$, which is comparable to that of the magnetite bulk [11]. A slight decrease in lattice parameter with increasing cobalt substitution is observed. It is known that iron and cobalt ferrites have the inverse spinel structure in which the divalent are on the octahedral site B and the trivalent ions are equally divided between the tetrahedral A and octahedral B sites. The variation in unite cell size may be attributed to the ionic radius of six-fold-coordinated $Co^{2+}$ being smaller (0.72 Å) than that of six-fold-coordinated $Fe^{2+}$ (0.74 Å) [12]. The broad XRD lines indicate that the particles are in nanoscale. The peaks of (1 1 1), (2 2 0), (3 1 1), (2 2 2), (4 0 0), (4 2 2), (5 1 1) and (4 0 0) have been deconvoluted to Lorentzian curves for the determination of the crystallite size using full-width at half-maximum value. The crystallite size of the nanocrystalline samples were measured from XRD line broadening analysis applying Scherrer's formula [13]:

$$d = \frac{k\lambda}{\beta \cos\ \theta} \tag{1}$$

where $d$ is the dimension of the crystallites, $\lambda$ the wavelength of the X-ray radiation, $\theta$ the Bragg angle, $k$ a shape factor taken to be 0.94 and $\beta$ the peak width measured at half of the maximum intensity. The calculation showed that the mean crystallite size values $\langle d_{XRD}\rangle$ of the samples are 9.5–11 nm.

The shape, size and morphology of the particles were examined by direct observation via transmission electron microscopy. The TEM micrographs for the samples are given in the left column of Fig. 2. The observations reveal that the particles are approximately spherical in shape and agglomerated. A small portion of tiny particles can be observed surrounding the larger crystals. The particle size histograms obtained from sampling of about 600 particles from different TEM graphs for each sample are presented in the right column of Fig. 2. The particle size data were modeled with the log-normal distribution function to estimate the average particle size $\langle d_{TEM}\rangle$. The $\langle d_{TEM}\rangle$ values are listed in Table 1 with the standard deviation $\sigma(\ln(d_{TEM})) = 0.15$, 0.17 and 0.22 for the samples S0, S02 and S04, respectively.

**Table 1**
Cobalt content $x$, lattice constant $a$, mean crystallite size $\langle d_{XRD}\rangle$, mean particle diameters $\langle d_{TEM}\rangle$ and $\langle d_{mag}\rangle$ as determined, respectively, from TEM measurements and from Langevin fits to the magnetization curves at 300 K (Eq. (2)) for the $Co_xFe_{3-x}O_4$ nanoparticle samples.

| Sample | $x$ | $a$ (Å) | $\langle d_{XRD}\rangle$ (nm) | $\langle d_{TEM}\rangle$ (nm) | $\langle d_{mag}\rangle$ (nm) |
|---|---|---|---|---|---|
| S0 | 0 | 8.398 | 9.5 | 9.8 ± 0.1 | 10.5 ± 0.1 |
| S02 | 0.198 | 8.396 | 10 | 10.1 ± 0.1 | 9.6 ± 0.1 |
| S04 | 0.416 | 8.394 | 11 | 11.7 ± 0.3 | 11.5 ± 0.1 |

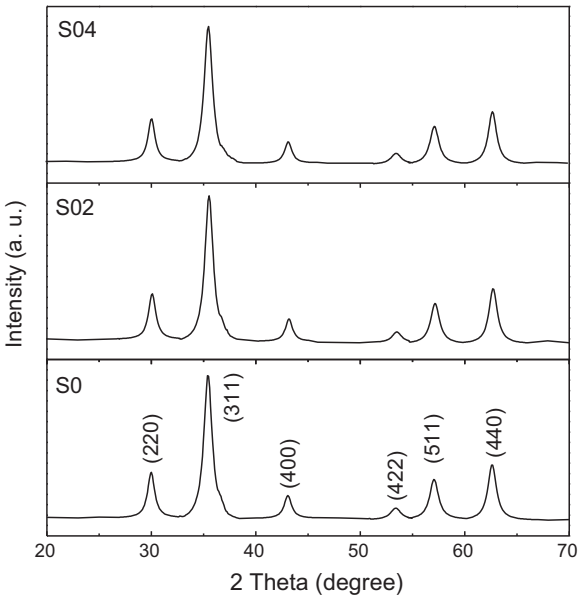


**Fig. 1.** Indexed XRD patters of the $Co_xFe_{3-x}O_4$ nanoparticle samples.

### 3.2. Magnetic characterization

The hysteresis loops of the fixed powder samples were measured from 100 K to room temperature. At 100 K, the hysteresis loops show a coercivity $H_c$ and a magnetic remanence $M_r$ (Fig. 3a). With increasing temperature $H_c$ and $M_r$ decrease and vanish as the samples change from ferri- to superparamagnetic state. The $M$–$H$ loops at 300 K are shown in Fig. 3b which exhibits the superparamagnetic behavior of the samples. From the hysteresis curves in the ferrimagnetic state, the values of $H_c$, $M_r$ and $M_s$ were deduced. The saturation magnetization was determined by plotting $M$ versus $1/H$ at high fields and determining the infinite field value through extrapolation. For the hysteresis curves in the superparamagnetic region, it is possible to fit the data to a modified Langevin function:

$$M(T,H) = M_s\left(\coth\left(\frac{M_s\rho\pi(\langle d_{mag}\rangle^3/6)}{k_BT}\right) - \frac{k_BT}{M_s\rho\pi(\langle d_{mag}\rangle^3/6)}\right) + \chi H \tag{2}$$

where $M_s$ is the saturation magnetization in electromagnetic unit per gram, $\pi(\langle d_{mag}\rangle^3/6)$ the mean magnetic volume of the particles, $\rho$ the mass density of the particles, and $\chi$ represents a linear susceptibility term associated with paramagnetic contributions from impurities and possible disordered spins at the particle surfaces which becomes significant in high external magnetic fields. The mass density was determined via the relation $\rho = 8M/(N_Aa^3)$ where $M$ is the mole mass in gram, $a$ the lattice constant and $N_A$ the Avogadro constant. In all fits $\chi$ was approximately $10^{-4}$ emu/g Oe. The mean magnetic diameter values $\langle d_{mag}\rangle$ for each sample at different temperatures was found to be very close to one and another. As indicated in Table 1, the average values $\langle d_{mag}\rangle$ are in fair agreement with those determined via XRD and TEM measurements. The

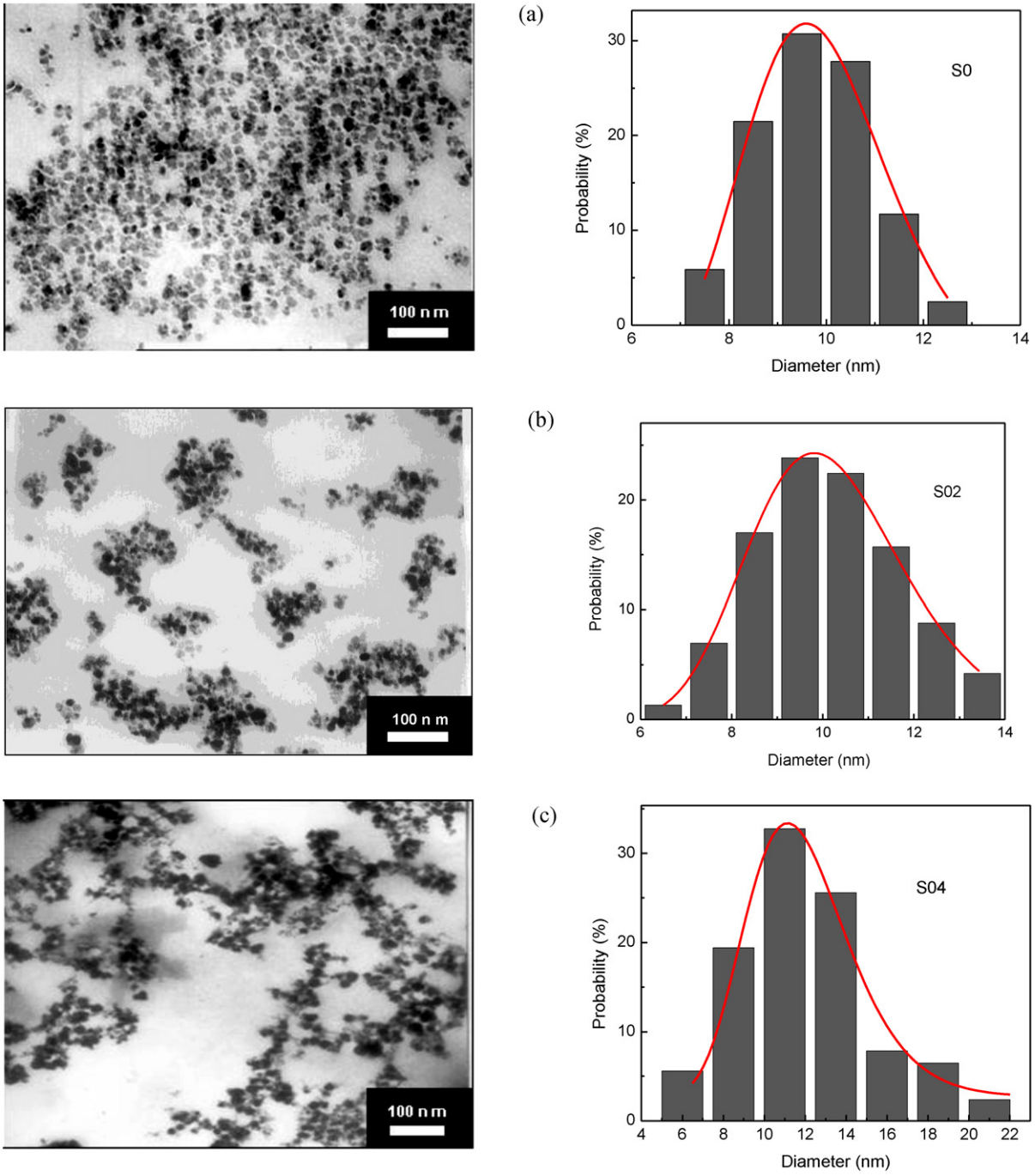


**Fig. 2.** Transmission electron micrographs (left) and histograms of the particle size distribution (right) for the $Co_xFe_{3-x}O_4$ nanoparticle samples S0 (a), S02 (b) and S04 (c). The solid curves are the fits to the lognormal distribution function.

$M_s$ values in superparamagnetic region were also deduced from the fits to Eq. (2).

The saturation magnetization of the samples as a function of temperature is shown in Fig. 4. These data can be fitted by a modified Bloch law:

$$Ms(T) = Ms(0)[1 - BT^{\alpha}] \quad (3)$$

where $M_s(0)$ is the saturation magnetization at 0 K, $B$ is the Bloch's constant and $\alpha$ the Bloch exponent. For infinitely large ferro/ferrimagnetic systems, the temperature dependence of the saturation magnetization below about one of half of the Curie temperature follows the Bloch $T^{3/2}$ behavior which is the result of the spin-wave excitations [14]. The best fits to Eq. (3) yield the value $\alpha = 2.2$, 2.2 and 2.1 for the samples S0, S02 and S04, respectively. Similar results were observed for ultrafine metal and alloys particles and for different spinel ferrite nanoparticle systems [5,6,15–17]. Chen et al. [5] obtained $\alpha$ values in the range of 1.6–2.0 for $MnFe_2O_4$ particles with particle size varying from 5 to 15 nm. Maaz et al. [6] and Alves et al. [17] found $\alpha$ close to 2.0 for $NiFe_2O_4$ and $CuFe_2O_4$ nanoparticles, respectively. The deviation from the $T^{3/2}$ dependence observed in the ultrafine magnetic particles has been analyzed in details elsewhere and was accounted for several finite size effects such as an energy gap in the density of states of spin-waves and lack of magnetic coordination at the surfaces [15]. The saturation magnetization values at zero temperature $M_s(0)$ derived for our samples from the fits to Eq. (3) are presented

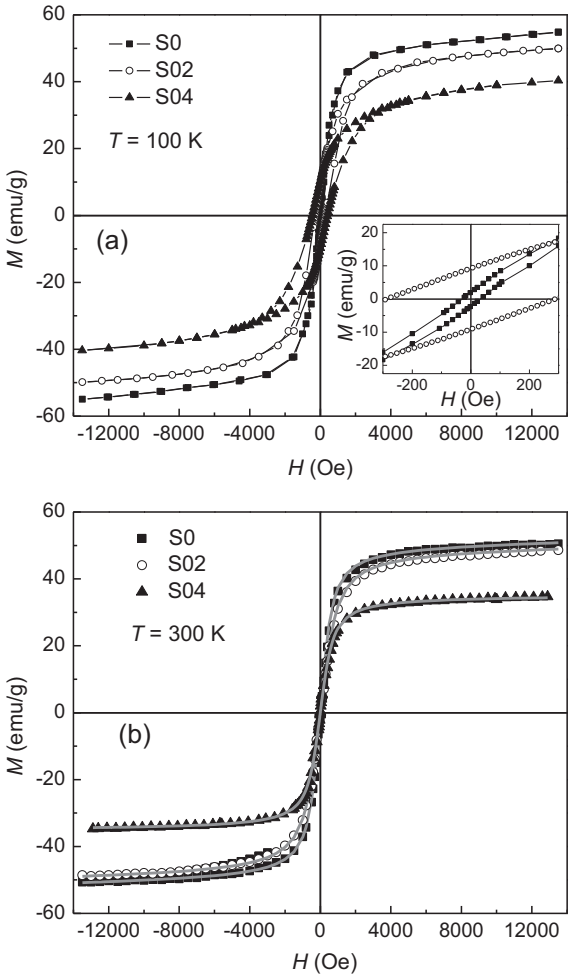


**Fig. 3.** (a) Hysteresis loops measured at 100 K for the $Co_xFe_{3-x}O_4$ nanoparticle samples. The inset shows the magnified region around the origin. (b) Hysteresis loops measured at 300 K for the $Co_xFe_{3-x}O_4$ nanoparticle samples. The solid curves are the fits to the modified Langevin function (Eq. (2)).

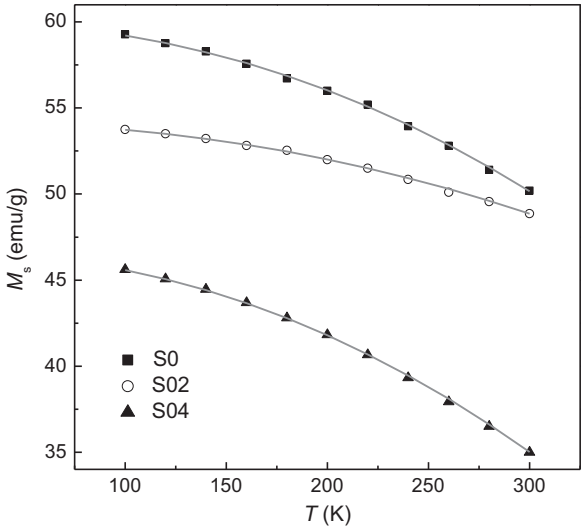


**Fig. 4.** Saturation magnetization $M_s$ as a function of temperature for the $Co_xFe_{3-x}O_4$ nanoparticle samples. The solid lines are the fit curves according to modified Bloch law (Eq. (3)).

**Table 2**
Magnetic parameters for the $Co_xFe_{3-x}O_4$ nanoparticle samples including Curie temperature $T_C$, blocking temperature $T_B$ and its mean value $\langle T_B \rangle$, interparticle interaction parameter $T_o$ and extrapolated magnetization at zero temperature $M_s(0)$. For comparison, the values of $M_s^{Néel}$ calculated based on the Néel model ($=M_B - M_A$) with the spin-only cation moments are also shown.

| Sample | $T_C$ (K) | $T_B$ (K) | $\langle T_B \rangle$ (K) | $T_o$ (K) | $M_s(0)$ ($\mu_B$/f.u.) | $M_s^{Néel}$ ($\mu_B$/f.u.) |
|---|---|---|---|---|---|---|
| S0 | 665 | 185 | 131 ± 1.4 | 70 | 2.41 | 4 |
| S02 | 660 | 205 | 129.9 ± 1.3 | 50 | 2.25 | 3.8 |
| S04 | 639 | 210 | 133.9 ± 2.0 | 80 | 1.95 | 3.6 |

in Table 2 in dimension of $\mu_B$ per chemical formula unit. Assuming the Néel model for ferrimagnetic order and the spin-only values of $Fe^{3+}$ ($5\mu_B$), $Fe^{2+}$ ($4\mu_B$) and $Co^{2+}$ ($3\mu_B$), the theoretical magnetic moments $M^{Néel}$ are also calculated for these samples based on the corresponding nominal composition with inversed cation distribution. It is found that the $M_s(0)$ values are 54–60% lower than $M^{Néel}$ values. Apart from the error in $M_s(0)$ due to the extrapolation between 0 K and 100 K, the lowered saturation magnetization can be originated from other sources, e.g. non- or weak magnetic impurities, adsorbed water at the particle surface, deviation from nominal composition and the existence of random canting of particle surface spins. In addition, the decrease in $M_s$ observed at all investigated temperatures with increasing cobalt content may be due to the occupation of B sites by the $Co^{2+}$ ions with lower spin moment.

In order to evaluate the effect of the interaction between nanoparticles in the fixed powder samples, initial susceptibility at various temperatures $\chi_i$ was determined as the slope of the $M$–$H$ curve with $H$ below 100 Oe. For magnetically interacting particles, in superparamagnetic region $\chi_i$ depends on temperature as [18]:

$$\chi_i \propto \frac{\mu^2}{3k_B(T - T_o)} \quad (4)$$

where $\mu$ is the magnetic moment per particle and $T_o$ is the interaction parameter. Fig. 5 shows $\chi_i^{-1}$ of the samples versus temperature. According to Eq. (4) the plot should lead to an almost straight line. Due to the fact that $\mu$ is dependent on temperature, the curve is not completely linear. Extrapolation to zero inverse susceptibility yields the values of $T_o$ which are shown in Table 2. Considerably high values of $T_o$ between 50 K and 80 K were obtained although the samples were dispersed in epoxy. The results indicate that interparticle interaction is non-negligible and must be

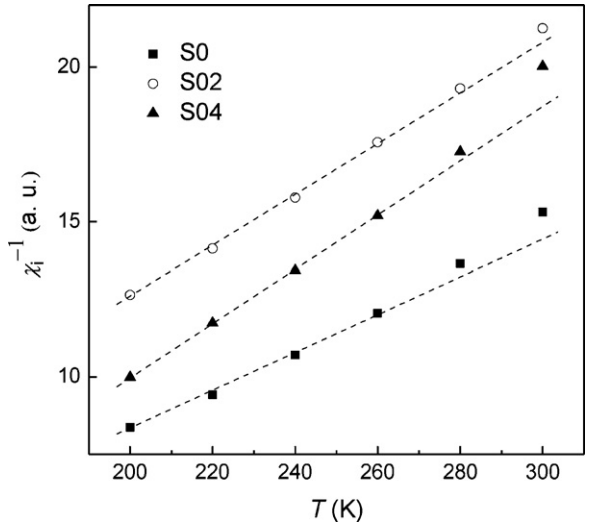


**Fig. 5.** Temperature dependence of the reciprocal initial susceptibility $\chi_i^{-1}$ for the $Co_xFe_{3-x}O_4$ nanoparticle samples.

considered during the analysis. It is noted, however, that the magnetization loops of the samples were measured at $T \geq 100$ K (Fig. 3) which is far higher than $T_o$ and in such conditions the thermal energy overcomes the interparticle interaction energy. The effect of the interaction between particles is therefore expected to have a negligible impact on the measured magnetization curves.

The blocking temperature $T_B$ can be approximated as the temperature where $H_c$ and $M_r$ decay to zero. In Figs. 6 and 7, the remanence relative to saturation magnetization $M_r/M_s$ and the coercivity $H_c$ of the three samples are plotted as a function of temperature. Superparamagnetic particles are also characterized by a maximum in the temperature variation of zero-field cooled magnetization measured in a small dc field. Zero-field cooled (ZFC) and field cooled (FC) magnetization curves were obtained for each sample at 50 Oe (Fig. 8). For the ZFC measurements, the samples were cooled from room temperature to 100 K, without any external magnetic field, and the magnetization was recorded while warming the samples in the applied field. For the FC curves, the samples were cooled in the applied field from room temperature to 100 K and

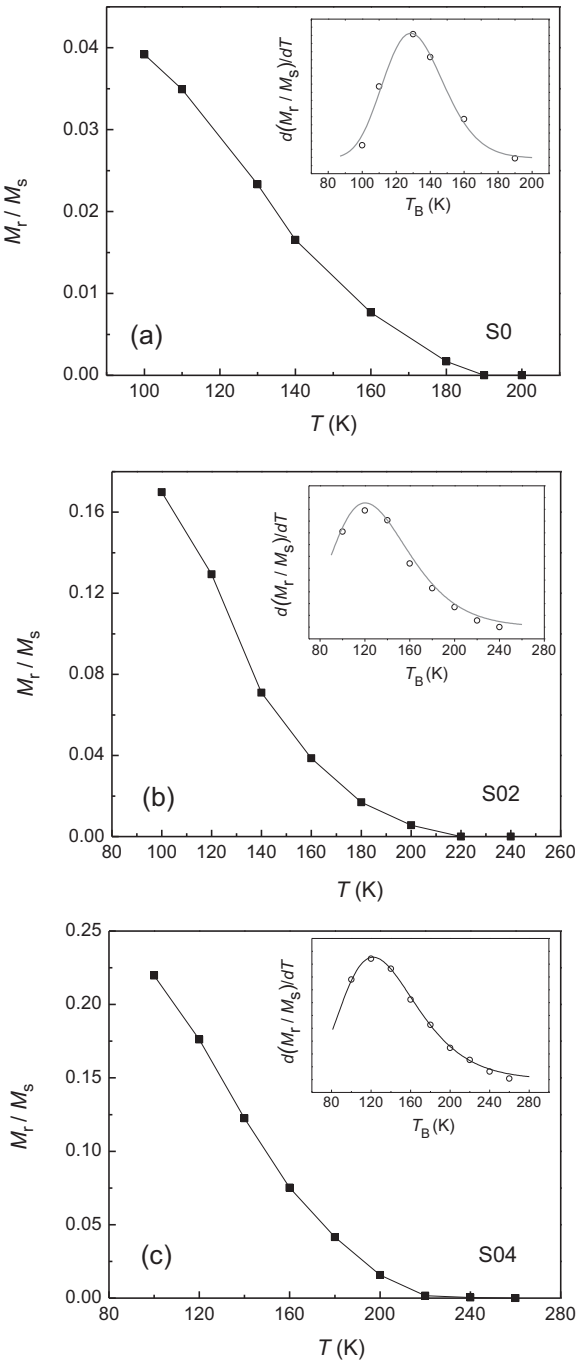


**Fig. 6.** The ratio of the remanence to saturation magnetization as a function of temperature for the $Co_xFe_{3-x}O_4$ nanoparticle samples. The solid lines are guides for the eyes. The insets show the derivative of $M_r/M_s$ versus temperature curves (Eq. (5)), and the solid curves are the best fits to a lognormal distribution of blocking temperatures.

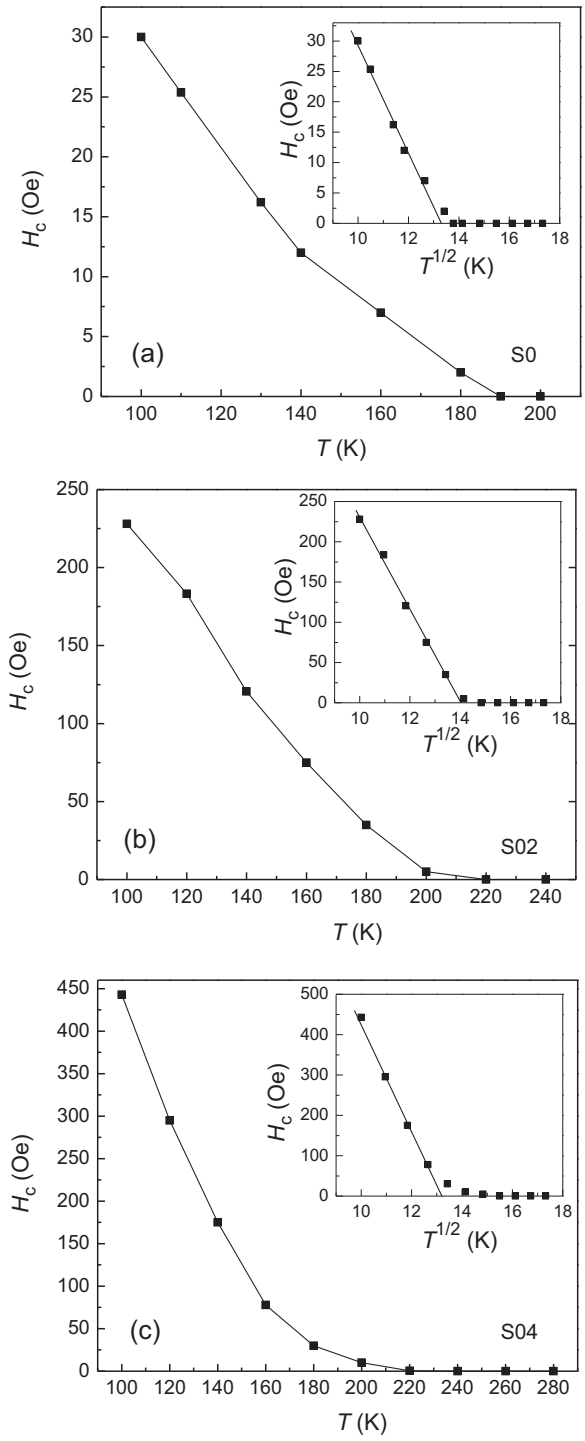


**Fig. 7.** Coercivity as a function of temperature for the $Co_xFe_{3-x}O_4$ nanoparticle samples. The solid lines are guides for the eyes. The insets show coercivity as a function of the square root of the temperature. The straight lines show the $T^{1/2}$ dependence (Eq. (7)).

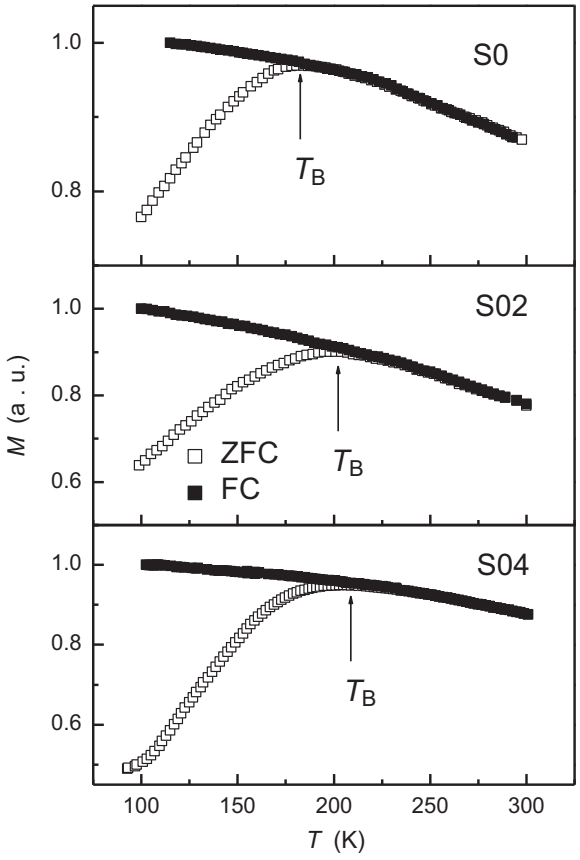


**Fig. 8.** ZFC and FC magnetization curves for the $Co_xFe_{3-x}O_4$ nanoparticle samples measured in an applied field of 50 Oe.

the magnetization was recorded in the same field with increasing temperature. Phenomenologically, the peak of the ZFC curves corresponds to a state where the particles cross from superparamagnetic behavior to ferrimagnetic behavior with decreasing temperature. As seen in Fig. 8, at low temperatures the magnetization in the FC curve is higher than that in the ZFC curve and the two curves overlap when the temperature rises above the blocking temperature. For the samples which have a particle size distribution, the temperature corresponding to the divergence between FC and ZFC curves is commonly referred to as the blocking temperature. The $T_B$ values derived from these measurements are in good agreement with those derived from the thermal decay of $H_c$ and $M_r$. The estimated $T_B$ values are listed in Table 1. On the other hand, it has been shown for ultrafine magnetic particles that the differential of the $M_r/M_s$ versus $T$ curve gives a direct measure of the distribution of blocking temperature [19], i.e.

$$f(T_B)\alpha\frac{d(M_r/M_s)}{dT}. \quad (5)$$

The distribution of blocking temperature is shown in the insets of Fig. 6. The full curves show the best fits of a lognormal distribution of blocking temperature. Since $T_B \propto KV$ [18], the distribution $f(T_B)$ reflects the variation of the particle size in the samples. The standard deviations $\sigma(\ln(T_B)) = 0.13$, 0.27 and 0.30 were obtained for the samples S0, S02 and S04, respectively. The data reveal that the substituted samples have a broader particle size range compared to the pure sample. The blocking temperature $T_B$ and its mean $\langle T_B\rangle$ values are shown in Table 2. It is observed that $T_B$ of the substituted samples are higher than that of the pure sample while their mean values $\langle T_B\rangle$ are very close to one and another.

The anisotropy constant was determined from the blocking temperature $T_B$. Using the Vogel–Fulcher law which describes the temperature dependence of the characteristic time for Néel relaxation that occurs through the rotation of particle's magnetic moment, the anisotropy constant was calculated via [20]

$$K = \frac{k_B(T_B - T_o)}{V} \quad \ln(\tau/\tau_0) \approx \frac{25k_B(T_B - T_o)}{V} \quad (6)$$

where $\tau$ is the time scale of the measurement and $\tau_0$ a characteristic time. For $\tau$, a value of 100 s is assumed and for $\tau_0$ a value of $10^{-9}$ s. It is noted that the anisotropy constant derived from Eq. (6) was already corrected for the effect of the interparticle interaction.

In the insets of Fig. 7, the coercivity $H_c$ is plotted as a function $T^{1/2}$. For monodisperse, non-interacting, uniaxial ferro/ferrimagnetic particles, the coercivity below the blocking temperature depends on temperature as [18]:

$$H_c = H_c^0\left[1 - \left(\frac{25k_BT}{KV}\right)^{1/2}\right] \quad (7)$$

where $H_c^0$ is the corecivity when the field is unaided by thermal energy. This relation is known as Kneller's law [21]. Based on the slope of the linear part of the $H_c$ versus $T^{1/2}$ curves, the anisotropy energy $KV$ in the investigated temperature range was also calculated via Eq. (7).

Table 3 presents the values of the anisotropy constants $K_{VF}$ and $K_{Kneller}$ determined by the above described methods. These values were calculated by using the mean particle volume $\langle V\rangle$ derived from the mean diameter $\langle d_{XRD}\rangle$ with assumption of spherical particle. It is noted that the mean particle volume $\langle V\rangle$ only slightly increases with increasing $x$ as observed via XRD broadening and TEM measurements. The obtained values were found to be in order of $10^6$ erg/cm$^3$. The $K_{VF}$ and $K_{Kneller}$ values agree quite well with each other for the substituted samples S02 and S04 whereas for the sample S0$K_{Kneller}$ is considerably larger than $K_{VF}$. The deviation between the anisotropy constant values for the sample S0 can be due to the fact that the material ($Fe_3O_4$) is not a uniaxial material [22] and therefore the determination of $K_{Kneller}$ via Eq. (7) may give a large error. On the other hand, the $K_{VF}$ value is in very good agreement with that determined by Calero-DdelC et al. [20] using the same method, i.e. via blocking temperature for $Fe_3O_4$ nanoparticles with diameter of 25 nm and dispersed in polymer with the mass ratios between particles and polymer of 0.1% and 1%. However, compared to the magnetocrystalline anisotropy constant of bulk $Fe_3O_4$ ($\sim 1\times10^5$ erg/cm$^3$) [22], the $K_{VF}$ value is still higher by a factor of 8. This observation suggests that the Vogel–Fulcher model may work well only for weak interaction [20] or there exists other anisotropy source, for instance from the surface with broken exchange bonds and modified chemical environment of the magnetic ions. For the substituted samples, the data are in the same order of magnitude with the anisotropy constants recently reported by Calero-DdelC et al. [10] for $Co_xFe_{3-x}O_4$ nanoparticles with diameters of around 3 nm and the cobalt contents in the range $x = 0.4$–0.6. It has been shown for bulk $Co_xFe_{3-x}O_4$ ferrites that substitution of iron by cobalt as low as 4 atomic percent leads to an increase of the first order magnetocrystalline anisotropy constant $K_1$ to above $3\times10^6$ erg/cm$^3$ and $K_1$ increases with further increasing the cobalt content [8]. On the other hand, the particles are in single domain state and most of them have a nearly spherical shape, hence the

**Table 3**
Anisotropy constants for the $Co_xFe_{3-x}O_4$ nanoparticle samples.

| Sample | $K_{VF}$ ($10^6$ erg/cm$^3$) | $K_{Kneller}$ ($10^6$ erg/cm$^3$) |
|---|---|---|
| S0 | 0.84 | 1.38 |
| S02 | 1.07 | 1.3 |
| S04 | 0.67 | 0.8 |

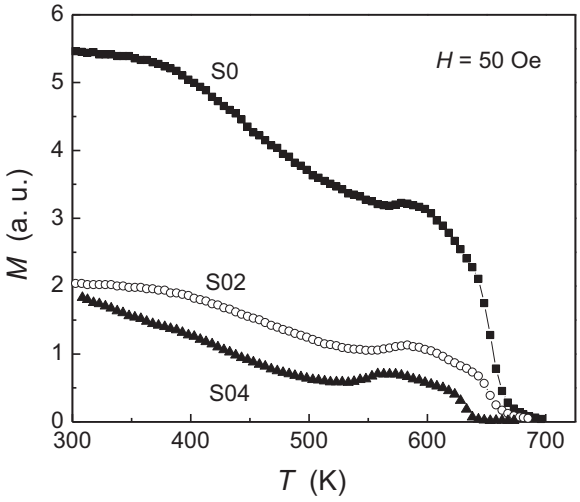


**Fig. 9.** Thermomagnetic curves for the $Co_xFe_{3-x}O_4$ nanoparticle samples measured in an applied field of 50 Oe.

shape anisotropy and stress anisotropy are negligible. The lower values of $K_{VF}$ observed for the cobalt substituted samples compared to the bulk magnetocrystalline anisotropy can be explained by the contribution of the surface anisotropy which may partly compensate the anisotropy of the particle's core or can be due to other reasons such as poor crystallinity or lattice defects. The two later factors may also account for the fact that, in comparison with the sample S02, the sample S04 has higher cobalt content but a lower anisotropy constant.

The Curie temperature of the samples in the forms of pressed pellets was investigated by thermomagnetization measurements. Fig. 9 shows the *M*–*T* curves of the samples measured in applied field 50 Oe. For all cases, the magnetization decreases with increasing temperature and a cusp appears in the curves at temperatures above ~550 K. The cusp in the *M*–*T* curve has been observed for similar systems which was attributed to the interaction between the nanoparticles in the samples [5,23,24] or grain growth effect as the samples were heated at high temperatures [25]. The Curie temperature $T_C$ is determined by the intersection of the tangent line at the largest slope with the horizontal axis. As summarized in Table 2, the Curie temperatures of the samples are about 200 K lower than that of $Fe_3O_4$ bulk (860 K) [8]. The decrease in Curie temperature compared to the bulk is usually observed in metal and oxide nanoparticles [5,15] and two-dimensional systems such as transition metal thin-film systems and rare-earth/nonmagnetic multilayers [26,27] and is explained by either finite size scaling or surface effect [28]. In addition, $T_C$ of the samples is also found to decease considerably with increasing the cobalt content which may be related to the lowering of the intersublattice exchange coupling between A and B sublattices. As reported previously for bulk ferrites [8], the exchange integral $J^A_{Fe^{3+}}-^B_{Fe^{2+}}$ between $Fe^{3+}$ ion in A lattice and $Fe^{2+}$ in B lattice is larger than $J^A_{Fe^{3+}}-^B_{Co^{2+}}$ between $Fe^{3+}$ ion in A lattice and $Co^{2+}$ in B lattice. This observation may support the fact that $Co^{2+}$ replaces for $Fe^{2+}$ in B sublattice in these cobalt substituted ferrite nanoparticles.

## 4. Conclusion

We have prepared cobalt-substituted ferrite nanoparticles by using aqueous phase coprecipitation method at reaction temperature slightly below room temperature. The size, shape and morphology of the particle samples were investigated. The particles are in the size range from few to about 22 nm with the mean diameter from 9.5 to 11 nm and have almost spherical shape. The magnetic measurements reveal remarkable influences of the finite size and surface effects and the cobalt substitution on the magnetic parameters of the samples including the saturation magnetization, Curie temperature, magnetic anisotropy energy and blocking temperature.

## Acknowledgment

The work was supported by Vietnam's National Foundation for Science and Technology Development (NAFOSTED) Grant no. 103.02.105.09.

## References

[1] S. Odenbach, K.H.J. Buschow (Eds.), Handbook of Magnetic Materials, vol. 16, Amsterdam, North-Holland, 2006, pp. 127–208.
[2] S.P. Gubin (Ed.), Magnetic Nanoparticles, Wiley-VCH Verlag, Weinheim, 2009 (Chapter 6).
[3] I. Safarik, M. Safarikova, Monatshefte für Chemie Springer-Verlag 133 (2002) 737–759.
[4] C. Bréschignag, P. Houdy, M. Lahmani (Eds.), Nanomaterials and Nanochemistry, Springer-Verlag, 2006 (Chapter 5).
[5] J.P. Chen, C.M. Sorensen, K.J. Klabunde, G.C. Hadjipanayis, E. Devlin, A. Kostikas, Phys. Rev. B 54 (9) (1996) 9288.
[6] K. Maaz, A. Mumtaz, S.K. Hasanain, M.F. Bertino, J. Magn. Magn. Mater. 322 (2010) 2199–2202.
[7] R.H. Kodama, A.E. Berkowitz, E.J. McNiff, S. Goner, Phys. Rev. Lett. 77 (4) (1996) 394.
[8] S. Krupička, P. Novák, E.P. Wohlfarth (Eds.), Ferromagnetic Materials, vol. 3, Amsterdam, North-Holland, 1982.
[9] C. Rath, S. Aand, R.P. Das, K.K. Sahu, S.D. Kulkarni, S.K. Date, N.C. Mishra, J. Appl. Phys. 91 (2002) 2211–2215.
[10] V.L. Calero-DdelC, C. Rinaldi, J. Magn. Magn. Mater. 314 (2007) 60–67.
[11] H.St.C. O'Neill, W.A. Dollase, Phys. Chem. Miner. 20 (1994) 541–555.
[12] W.D. Callister, Materials Science and Engineering. An Introduction, 7th ed., John Wiley & Sons, Inc., 2007.
[13] B.D. Cullity, Elements of X-Ray Diffraction, 2nd ed., Addison-Wesley, Reading, MA, 1978.
[14] C. Kittel, Introduction to Solid State Theory, Wiley, New York, 1971.
[15] P.V. Hendriksen, S. Linderoth, P.-A. Lindgård, J. Magn. Magn. Mater. 104–107 (1992) 1577–1579.
[16] S. Linderoth, L. Balcells, A. Labarta, J. Tejada, P.V. Hendriksen, S.A. Sethi, J. Magn. Magn. Mater. 124 (1993) 269–276.
[17] C.R. Alves, R. Aquino, M.H. Sousa, H.R. Rechenberg, G.F. Goya, F.A. Tourinho, J. Depeyrot, J. Met. Nanocrys. Mater. 20–21 (2004) 694–699.
[18] C.P. Bean, J.D. Livingston, J. Appl. Phys. 30 (1959) 120S–129S.
[19] R.W. Chantrell, M. El-Hilo, K. O'Grady, IEEE Trans. Magn. 27 (1991) 3570–3578.
[20] V.L. Calero-Diaz del Castillo, C. Rinaldi, IEEE Trans. Magn. 46 (2010) 852–859.
[21] B.D. Cullity, C.D. Graham, Introduction to Magnetic Materials, John Wiley & Sons, Inc., 2009.
[22] S. Chikazumi, Physics of Magnetism, Clarendon Press, Oxford, 1997, 289.
[23] S. Morup, F. Bodker, P.V. Hendriksen, S. Linderoth, Phys. Rev. B 52 (1995) 287.
[24] P. Bouchand, P.G. Zerah, Phys. Rev. B 47 (1993) 9095.
[25] W. Wolski, E. Wolska, J. Kaczmarek, P. Piszora, Phys. Status Solidi A 152 (1995) K19–K22.
[26] F. Huang, G.L. Mankey, M.T. Kief, R.F. Willis, J. Appl. Phys. 73 (3) (1993) 6760.
[27] M.J. O'Shea, P. Perera, J. Appl. Phys. 76 (3) (1994) 6174.
[28] K. Binder, Physica 62 (1972) 508–526.